Available online at www.sciencedirect.com

ScienceDirect

Advances in Space Research 54 (2014) 1530–1543

ADVANCES IN SPACE RESEARCH (a COSPAR publication)

www.elsevier.com/locate/asr

Langley method applied in study of aerosol optical depth in the Brazilian semiarid region using 500, 670 and 870 nm bands for sun photometer calibration

J.G. Cerqueira Jr. [a,b,*], J.H. Fernandez [b], J.J. Hoelzemann [b], N.M.P. Leme [a], C.T. Sousa [a]

[a] *Instituto Nacional de Pesquisas Espaciais – INPE, CRN – (National Institute for Space Research, Northeast Regional Center), Address: Rua: Carlos Serrano, 2073 – Lagoa Nova, Natal, RN 59076-740, Brazil*

[b] *Universidade Federal do Rio Grande do Norte (UFRN), Address: Campus Universitário UFRN; Av. Sen. Salgado Filho, 3000 – Lagoa Nova, Natal, RN 59078-970, Brazil*

Received 2 January 2014; received in revised form 13 May 2014; accepted 3 June 2014
Available online 21 June 2014

Abstract

Due to the high costs of commercial monitoring instruments, a portable sun photometer was developed at INPE/CRN laboratories, operating in four bands, with two bands in the visible spectrum and two in near infrared. The instrument calibration process is performed by applying the classical Langley method. Application of the Langley's methodology requires a site with high optical stability during the measurements, which is usually found in high altitudes. However, far from being an ideal site, Harrison et al. (1994) report success with applying the Langley method to some data for a site in Boulder, Colorado. Recently, Liu et al. (2011) show that low elevation sites, far away from urban and industrial centers can provide a stable optical depth, similar to high altitudes. In this study we investigated the feasibility of applying the methodology in the semiarid region of northeastern Brazil, far away from pollution areas with low altitudes, for sun photometer calibration. We investigated optical depth stability using two periods of measurements in the year during dry season in austral summer. The first one was in December when the native vegetation naturally dries, losing all its leaves and the second one was in September in the middle of the dry season when the vegetation is still with leaves. The data were distributed during four days in December 2012 and four days in September 2013 totaling eleven half days of collections between mornings and afternoons and by means of fitted line to the data V_0 values were found. Despite the high correlation between the collected data and the fitted line, the study showed a variation between the values of V_0 greater than allowed for sun photometer calibration. The lowest V_0 variation reached in this experiment with values lower than 3% for the bands 500, 670 and 870 nm are displayed in tables. The results indicate that the site needs to be better characterized with studies in more favorable periods, soon after the rainy season.

Keywords: Optical depth; Brazilian semiarid; Sun photometer calibration; Langley method

1. Introduction

The calibration of a sun photometer (SPM) using the Langley method (LM) for measuring the aerosol optical depth (AOD) is a well-established methodology known worldwide. This methodology avoids the need of calibration in the laboratory, making it unnecessary to create infrastructure and expensive calibration devices. The challenge

* Corresponding author at: Instituto Nacional de Pesquisas Espaciais – INPE, CRN – (National Institute for Space Research, Northeast Regional Center), Address: Rua: Carlos Serrano, 2073 – Lagoa Nova, Natal, RN 59076-740, Brazil.

E-mail addresses: jgcjunior@crn2.inpe.br (J.G. Cerqueira Jr.), jhfernandez@ect.ufrn.br (J.H. Fernandez), judith.hoelzemann@ect.ufrn.br (J.J. Hoelzemann), nleme@crn.inpe.br (N.M.P. Leme), cristina.tsr@crn.inpe.br (C.T. Sousa).

http://dx.doi.org/10.1016/j.asr.2014.06.006
0273-1177/

of this methodology is to identify sites with optimal conditions i.e., highly stable optical depth of the atmosphere that is associated with low AOD.

According to Shaw (1983), in order to measure the optical depth, the photometer needs a narrow view angle to the sun. This narrow bandwidth is necessary for measuring only direct radiation, thus avoiding the interference of diffused radiation. Generally, the sites chosen for SPM calibration are located at high altitudes, because of their larger distance to the lower troposphere, where the main sources of natural or anthropogenic aerosols are located. Usually, sites with lower air density have a larger optical stability due to weak absorption and scattering of solar radiation that remain proportional to the optical air mass variation.

At high altitudes during the majority of calibration periods, the interference of clouds is also avoided. The MLO (Mauna Loa Observatory), that belongs to NOAA (National Oceanic and Atmospheric Administration), located in Hawaii – USA, at 3400 m, and also the observatory on Mount Jungfraujoch, in the Swiss Alps, at 3600 m, are examples of sites where low AOD for calibrating the sun photometers can be found.

However, studies show that sites located in areas of low and medium altitude, distant from natural or anthropogenic sources of pollution, can achieve sufficient optical stability in the atmosphere to obtain calibration coefficients (Harrison et al., 1994). According to Liu et al. (2011) the correlation of the data obtained with the MRSBR (Multiband Radiometer with Blade Rotary Shadowing) calibrated at low altitudes had a correlation coefficient of 0.97, compared with the photometer of AERONET (AErosol RObotic NETwork). Therefore, with the given topographic condition in lowlands it is possible to successfully use the Langley method.

In regions without pollution sources, the convective processes in the air and wind speed are the factors that can cause instability of the atmospheric optical depth. The convections process starts with the heating of the air near the ground and creates warm air masses that rise into the troposphere, transporting aerosols. The aerosol transportation changes the density of particles in the atmosphere thus becoming the main cause of optical instability. This optical instability is perceived by the photometer by variation in the level of solar radiation due to scattering and absorption that reach the planet's surface.

For this study we used the SPM FSM-4 (Solar Multiband Photometer with 4 channels), which is a small portable device, manually operated, mounted on a tripod. Developed in the laboratories of INPE – CRN (Instituto Nacional de Pesquisas Espaciais – Centro Regional do Nordeste), the work's main objective was the acquisition of a technology to construct and calibrate a low cost solar photometer without sacrificing the accuracy of the measurements for this type of device.

This work is organized in the following sequence: first we present in Section 2, the applied techniques (theory equations and strategies) for the photometer's calibration. The FSM-4 construction details are shown and a comprehensive explanation in Section 3 and also about the software designed to work with collected data during instrument operation is presented. In Section 4 the data collected with the FSM-4 at the studied site are presented, as well as the methodology applied in the variability study of the calibration constants and results.

2. The Langley method

The attenuation of solar radiation by the terrestrial atmosphere is represented by Beer's law (Eq. (1)). This law is only valid for a monochromatic source (Liou, 2002 and Halthore et al., 1997):

$$V_\lambda = V_0 \left(\frac{D_{Day}}{D_{min}}\right)^2 e^{-(\tau_{Aer}+\tau_R+\tau_{Gas}+\tau_{O_3})m} \quad (1)$$

where V_λ, given in millivolt (mV), corresponds to the photon conversion factor voltage with the influence of the atmosphere; V_0, which is also given in millivolt (mV) is the photon conversion factor voltage without the influence of the atmosphere, that is, it simulates the sun photometer measurements at the top of the atmosphere, and is known as the extraterrestrial constant; D_{Day} and D_{min} are the Earth–Sun distances at the present day of measurement and at minimum possible distance, respectively. Thus, the D_{min} corresponds to the perihelion, which is the closest point in the Earth–Sun orbit (1 AU – astronomical unit), equal to 1.47×10^{11} m.

It is considered that a bandwidth of 10 nm filter is within the maximum limit for the application of this law. Several global networks of photometers, including AEROCAN (Aerosols in Canada) and AERONET (AErosol RObotic NETwork) NASA (National Aeronautic and Space Administration) use filters with 10 nm bands. These networks use the Langley method, which is derived from Beer's Law, for calibration (McArthur et al., 2003).

The optical air mass (m) can be defined as all elements, i.e., gases and aerosols, encountered along the course that solar radiation takes through the atmosphere until reaching the surface of the planet. The atmospheric optical depth given by "τ", is caused by Rayleigh scattering (τ_R) and absorption of gases (τ_{Gas}), such as ozone (τ_{O_3}) and aerosols (τ_{Aer}), and AOD is the total extinction, namely, scattering and absorption by aerosols (WMO, 2008). This work was carried out using the methodology of Kasten and Young (1989) to correct the optical air mass for large zenith angles due to the curvature of the atmosphere that accompanies the curvature of the planet. We created a computer program SODDA-MOP (Software Debugger Data – Optics air Mass) that makes use of this methodology and is presented in Section 3.1.2.

The Langley method allows the measurement of atmospheric transmittance (Reagan et al., 1987, 1992; Bruegge et al., 1992). This method consists in linearization of Eq. (1)

placing it in a logarithmic form, and then transforming it into an equation of the fitted line $y = b - ax$, as shown in Eq. (2) below:

$$\ln V_\lambda - \ln \left(\frac{D_{Day}}{D_{min}}\right)^2 = \ln V_0 - \tau_{total} m \quad (2)$$

Therefore, x, y, a, and b can be defined as:

$$x = m \quad (3)$$

$$y = \ln V_\lambda - \ln \left(\frac{D_{Day}}{D_{min}}\right)^2 \quad (4)$$

$$b = \ln V_0 \quad (5)$$

$$a = \tau_{total} \quad (6)$$

In Eqs. (3)–(6), "x" and "y" are variables, "b" is the extraterrestrial calibration constant, and "a" is the total optical depth (coefficient angle), respectively. Plotting a graph of m versus $\ln V_\lambda - \ln (D_{Day}/D_{min})^2$ and the extension of the fitted line using linear regression by the least squares method we obtain the value for $m = 0$, i.e., the extraterrestrial constant of the device for the band as given by $\ln V_0$.

Simulation with a radiative transfer model like MODTRAN-3 (MODerate resolution atmospheric TRANsmission) shows that for a solar zenith angle of 60°, the effective attenuators of solar energy in the 0.2–5 μm region in attenuation decreasing order of importance are Rayleigh scattering (15%), ozone (3.5%), carbon dioxide (1.2%), oxygen (0.8%), methane (0.3%), nitrogen oxide (0.13%), nitrogen dioxide (0.12%), nitrous oxide (0.11%), sulfur dioxide (0.1%) and carbon monoxide (0.01%) (Halthore et al., 1997).

According to Rollin (2000), the effect of mixed gases in the atmosphere is constant, but the photometers, including ours (the FSM-4) and the CIMEL photometer of the AERONET network, use bands that are not influenced by those, therefore the contribution of these gases to the optical depth (τ_{gas}) can be neglected and only aerosols are accounted for.

For cloudless and clear days it is possible to determine an average optical depth from the slopes of the fitted lines to the data without knowing the $V_{0\lambda}$ constant, (Schmid and Wehrli, 1995). Eq. (7) shows the total optical depth that is given by the sum of the optical depth of ozone, other trace gases, and the Rayleigh scattering (Green, 1964):

$$\tau_{total} = \tau_{Aer} + \tau_{gas} + \tau_{O_3} + \tau_{Ray} \quad (7)$$

$$\tau_{Aer} = \tau_{total} - (\tau_{O_3} + \tau_{Ray}) \quad (8)$$

Therefore, the AOD (τ_{Aer}) is given by Eq. (8), thus leading to Eq. (9):

$$\tau_{Aer} = \frac{1}{m}\left(\ln V_0 - \ln V_\lambda + \ln \left(\frac{D_{Day}}{D_{min}}\right)^2\right) - \tau_{O_3} - \tau_{Ray} \quad (9)$$

With the calibrated device it is possible to calculate the AOD with Eq. (9). This equation guarantees a calibrated device, that is, with an extraterrestrial calibration constant that permits a successful instantaneous AOD calculation.

The calculation of optical depth for ozone is given by Eq. (10) (Silva and Kirchhoff, 2004). Using Eq. (10) to calculate optical depth in the ozone Chappuis band, ranging from 450 to 850 nm, gives us:

$$\tau_{O_3} = \sigma \times DU \times 2.69 \times 10^{16} \quad (10)$$

σ is the ozone absorption cross section, DU is the ozone concentration expressed in Dobson Units and 2.69×10^{16} are the thousandth of the Loschmidt number. Sahai et al. (2000) show that stratospheric ozone over northeastern Brazil ranges between 255 and 275 DU, and these measurements were taken in the city of Natal, in the state of Rio Grande do Norte (RN), Brazil. Therefore, the present measurements were conducted in the city of Caicó–RN, which is less than 280 km from Natal, and values of stratospheric ozone can be expected to be similar.

The seasonal variation of stratospheric ozone had no influence on the calculation of the optical depth, since it changes less than 0.001 in optical depth for ozone in the 500 and 670 nm bands. In our study the ozone average value 265 DU to calculate the ozone optical depth was used with a precision of 3 decimal places (10^{-3}), as used in the AERONET project, which is sufficient for the accuracy of AOD measurements.

In a recent study conducted by Serdyuchenko et al. (2011) an accurate survey of the ozone cross section was made. For the present study we chose ozone cross section values for the absorption bands of 500 nm and 670 nm of 1.18×10^{-21} cm^2/molecule and 1.67×10^{-21} cm^2/molecule, respectively. These are average values for different temperatures. For these data the following values were obtained:

$$\tau_{O_3(500\ nm)} = 0.008 \qquad \tau_{O_3(670\ nm)} = 0.012$$

As cited by Kaufman (1993), the AOD is calculated by subtracting the Rayleigh scattering and absorption from the overall ozone optical depth. According to Shaw (1983) the uncertainties to the calibration of a photometer using the method of Langley are, to first order, proportional to the value of the AOD. The ozone contribution to the total optical depth varies between 10% and 20% for the Chappuis band, and contributes with values between 0.1 and 0.2, which is typical for rural areas at low altitude.

Rayleigh scattering is another important factor to be taken into account in calculating the AOD. The Rayleigh scattering occurs when the incident electromagnetic radiation with wavelength "λ" collides with particles smaller than 0.1λ radius, in most of the cases atoms and molecules (Liou, 2002).

The value of Rayleigh scattering was calculated following Robinson (1966) using Eq. (13), and subsequently corrected by Young (1981) and used by Dutton et al. (1994) to calculate the Rayleigh optical depth. An inaccuracy in this

formula is cited by Bodhaine et al. (1999), especially for the UV band, due to the difference of the exponent in this spectrum range. This fact does not invalidate Eq. (13), since the study was done in the visible and NIR spectrum. A comparison of the Rayleigh optical depth in Bodhaine et al. (1999) with our calculated values following Eq. (11) show similar results for the 500 nm band, 670 and 870 nm with an accuracy of ±0.001 (±0.5%) optical depth, as desirable for this study. The Rayleigh optical depth was calculated following:

$$\tau_{Ray}(\lambda) = 0.00877\frac{P}{P_0}\lambda^{-4.05} \quad (11)$$

where P is the pressure at the measurement site, P_0 is the atmospheric pressure at sea level (1013.25 hPa) and λ is the wavelength in micrometer (μm).

During our measurement campaigns, pressure ranged between 992 and 998.5 hPa. For these values of atmospheric pressure the Rayleigh optical depth for the bands 500, 670 and 870 nm were, respectively:

$$\tau_{Ray(500\ nm)} = 0.143 \quad \tau_{Ray(670\ nm)} = 0.044$$
$$\tau_{Ray(870\ nm)} = 0.015$$

3. The FSM-4 sun photometer

To acquire instrumental technology a multi-band portable solar photometer, the FSM-4, operating on the bands in Table 1, was developed.

The 940 nm band exhibits strong absorption by water vapor, and is usually used only for obtaining the PWC (Precipitable Water Column), (Bruegge et al., 1992). However, the 940 nm band may only be used with the modified Langley method for calibration, and is thus not considered in the present study, but will be investigated in separate paper.

The instrument development focused on the search for test materials, the technical construction, finalizing with the testing of the calibration methodology. The goal was to receive a more affordable device than the imported ones, easily operated, portable, and with good accuracy in the data.

The design of the collimation tube for solar radiation follows the standard WMO (2005) viewing angle for a device used in measuring direct solar radiation i.e., FOV (Field Of View) with 2.5° degree. The opening angle of the FSM-4 photometer was designed according to Slusser et al. (2000), and operated over a tripod to more stability. The sensor (photodiode) demonstrated thermal stability with about 1.5% variation in the output signal for 10 °C of ambience temperature variation i.e., the conversion factor versus photon output voltage has low values compared to those found in the Langley calibration methodology. A similar project developed by Kobayashi (1981) shows good temperature stability for silicon photodiodes operating between 28 °C and 45 °C, with a temperature variation coefficient of 0.15 mV/°C.

Table 1
Filters used in SPM – FSM-4.

Spectral band	500 nm	670 nm	870 nm	940 nm
Bandpass	10 nm	10 nm	10 nm	10 nm

The other sensitive element is the optical filter of the instrument. For the prototype filters with the spectral band shown in Table 1 were used, produced by the Andover Corporation. Each filter is specified by a calibration curve with bandwidth, attenuation factor within the band and coefficient of temperature variation.

The schematic diagram of the FSM-4 is shown in Fig. 1. The signal from the photodiode is amplified by a circuit, consisting of components used in instrumentation and powered by a DC/DC converter for high stability and a lithium battery as power source. Preliminary tests of the electromagnetic compatibility (EMC) show that this system is immune to medium and low interference, causing no change in the output signal.

To store the data a Campbell CR10-X datalogger was used. It is a robust device with high precision and widely used in scientific data measurement. The datalogger was placed in a separate box with its own power system and sealed rechargeable batteries. A computer program was created in the specific device language, which allows recording the data of the four channels of the FSM-4 and the temperature sensor, along with hours, minutes, seconds, and Julian day. Data is sampled on datalogger every second, while the operator holds the button "HAB". Measurements were interrupted when clouds were approaching the radiation path to avoid the measurement of incorrect optical depth values.

3.1. Software development

As data processing support a number of programs were developed in "C" programming language: SODDA-VALG (Software Debugger Data for Average Algorithm to maximum Value) and SODDA-MOP (Software Debugger Data to Optical air mass).

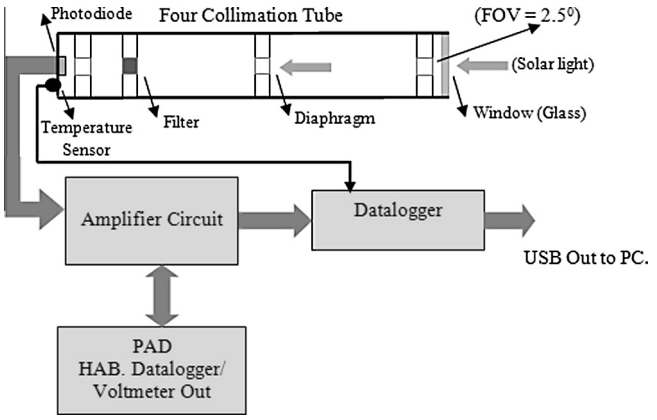

Fig. 1. FSM-4 – Schematic diagram.

3.1.1. SODDA-VALG software

The computer program SODDA-VALG selects within each minute the maximum voltage value among all values measured by the device. The selection of maximum values is performed in each of the four bands in which FSM-4 operates.

Data are collected during intervals of two or three minutes, the pointing device for at least 30 s to direct sun. As manual pointing to the sun does not provide the same accuracy as an automatic pointing system, a large number of measurements help eliminating this potential pointing error. To best fit the collected data an algorithm was created that uses multiple maximum values during the measurement time, to obtain average and the standard deviation, thus discarding bad data due to incorrect pointing to the sun. This extended appointment also helps to correct signal degradation due to eventual unnoticed clouds at high altitudes that cross the photometer's line of sight.

This procedure was adopted in order to choose the most correct data where the appointment provides the highest value, thus preventing data to be distorted by thin invisible high clouds. The change in optical depth occurs smoothly during small time intervals. According to Smirnov et al. (2000), the optical depth variation within 1 min for clean air and for any wavelength at $\tau_{aer} < 0.7$ will be less than 0.02 in absence of clouds. According to Porter et al. (2001), the pointing errors to the sun and imperceptible clouds are among the largest sources of uncertainty in the portable Microtops sun photometer. Thus, it is necessary to quickly perform many successive measurements to ensure a better result.

For this reason, the uncertainty can be considered as similar to that resulting from data collected with the SPM, because they are similar device. The AERONET photometer network uses similar procedures for data selection, in this case not to avoid pointing errors, but to prevent measurements from being contaminated by clouds. Three measurements are made within one minute to compare the variation of the AOD values according to AERONET algorithm.

3.1.2. Software SODDA-MOP

After using SODDA-VALG the data is processed by SODDA-MOP. The correspondence between the value of the optical air mass and the maximum value collected is made by the SODDA-MOP program, which creates a table to generate the plots.

The air mass is that portion of the atmosphere on the vertical route that the solar radiation takes from the top of the atmosphere to the surface of the Earth. Osterwald and Emery (2000) show the optical air mass "m" calculated using the model proposed by Kasten (1966), Kasten and Young (1989) in Eq. (12):

$$m_a = \frac{P}{1013.25}\left[\cos\theta_z + 0.15(93.885 - \theta_z)^{-1.253}\right]^{-1}, \qquad (12)$$

where the solar zenith angle is θ_z, P is the local atmospheric pressure in hectopascal (hPa), and considering pressure at sea level at 1013.25 hPa.

The software uses the algorithm of the solar zenith angle θ proposed by Michalsky (1988) with accuracy in the order of ± 0.01 degrees valid from year 1950 to 2050.

Zenith angles of the small to moderate "m" may be regarded as $1/\cos\theta$ according to Alexandrov et al. (2007). Angles are considered as moderate when $\theta \leqslant 30$, considering a plane parallel atmosphere.

4. Experiment results and discussion

4.1. Location, period and meteorological data measurement

There were two campaigns to obtain the first data with a sun photometer in this region. The first campaign occurred from December 19–22, 2012, and the second one from September, 4–7, 2013. The experiment was accomplished in Caicó city that is located in the Brazilian semiarid region, which presents endemic vegetation similar to savanna. It is located at 6° 30′ 27″ S, and 37° 5′ 18″ W, at an altitude of 164 m. The local climatology shows no major variations in temperature, relative humidity or air pressure during the dry season which runs from July to December, with little or no rainfall. Fig. 2 shows the variability of the average monthly temperature and rainfall.

These data show that campaigns with four days duration, conducted in December 2012 and September 2013, are sufficient to characterize the variability of the optical depth of the local atmosphere due to the weather of the region, allowing their correct evaluation during dry season. The temperature is a climatic factor that can have great influence on the performance of the AOD due to convective force. However, the maximum and minimum temperature variability of monthly average is very small, and may be considered constant for all periods of the year. The cloudiness factor may hinder calibration campaigns at various times of the year. The main rainy season takes place from January to June, so the most propitious period for campaigns ranges from the months of July to December.

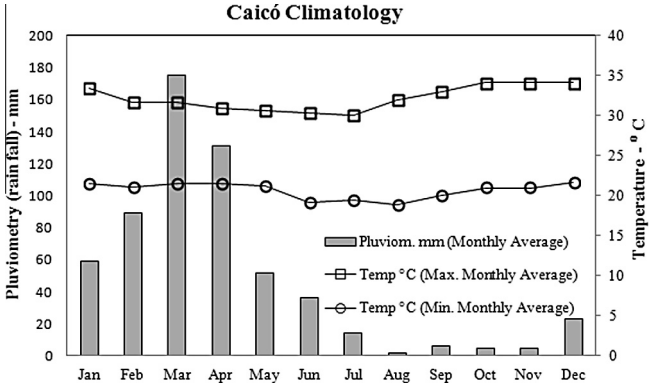

Fig. 2. Annual climatology in Caicó/Brazil.

September was chosen, as a month when local vegetation is still with leaves and also the month of December, when all the local vegetation loses its entire leafage. The climatic behavior does not change during this period, making long campaigns unnecessary for AOD characterization.

The Brazilian semiarid region showed in Fig. 3 does not have intense human activity that can significantly increase the optical depth of the region. Large industrial centers with polluting activities or even large-scale agriculture are virtually nonexistent. The region only has big centers of agricultural products with irrigation in places where large water reservoirs or rivers such as Petrolina/Brazil. However, the deforested vegetation is used to produce coal that will be utilized in ceramic production. The pollution due to vegetation fires occurs at very local points and can thus be neglected. The slow recovery of native vegetation due to climatological conditions of the area has led to areas with signals of desertification, or sparsely vegetated areas and exposed soil. This type of soil may increase the local increase in the AOD dust emissions caused by wind and convection of air masses.

Data were measured during the morning at sunrise and at afternoon, just before sunset, i.e., the values of the optical air mass range between 12 and 2, between 5:30 and 7:15 am local time (8:30 and 10:15 am UT) and between 3:40 and 5:30 pm local time (6:40 to 8:30 pm UT). According to Porter et al. (2001) measurements made between optical air mass values of two to five are sufficient for a good calibration. For this methodology, optical air mass values less than 2 were not used because solar radiation variation is very weak, becoming undetectable by the instrument which may generate errors during the line fitting. The variation of the optical air mass from two to one takes almost four hours and provokes an accumulation of measurements. Due to the uncertainty this may cause a change to the fitted line.

The campaigns of December, 19 to 22 – 2012 and September, 04 to 07 – 2013, proved to be quite productive, resulting in good determination coefficients, i.e., R^2 better than 99% in the lines fitted to the acquired data set, in majority sampling periods. The morning measurements periods are better than afternoon periods owing to a possible increase in aerosol brought by convective air masses, triggered by higher soil temperature, Shaw (1983). The temperature and relative humidity variations during the measurements periods (morning and afternoon) in December 2012 and September 2013 are shown in Table 2. Due to unavailability of local meteorological parameters in a better time resolution, the relative humidity and temperature were considered constant, i.e., the value obtained was used at 7 hs (Local time) (10 am – UT) and 15 hs (Local time) (6 pm – UT).

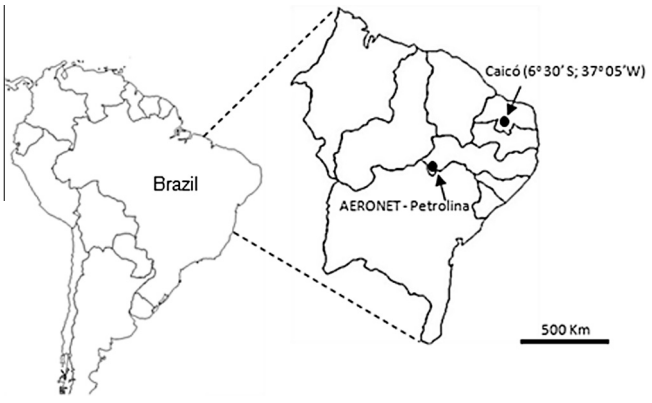

Fig. 3. Experiment location – Caicó/Brazil and AERONET/NASA in Petrolina/Brazil.

In Fig. 4 the wind speed average and its high great temporal variability at the site is shown. All this data were obtained from a Climatology station that belongs to INMET (Brazilian Meteorological Institute) located at UFRN (Federal University of RN State) in Caicó city. The climatological station's data are collected at 10 am, 6 and 24 pm (UT). The photometer's operation time range is marked in Fig. 4, as filled black markers (▲). The wind conditions found in September 2013 also showed similar conditions, i.e., temporal variability with medium ranging from 3 to 4 m/s.

4.2. Uncertainty estimates in FSM-4 measurements

According to Shaw (1979) the data uncertainty in a sun photometer must be calculated by observing three types of errors, namely: (a) Instrumental Errors, (b) Calibration Errors, (c) Errors imposed by the atmosphere. However, this work will not treat instrumental calibration, or even errors imposed by the atmosphere. As stated previously, this study main objective is solely an analysis of the AOD stability to characterize the atmosphere by the LM. The present data uncertainty analysis will consider only the errors related to the device logical functioning.

The data uncertainty in this experiment comes basically from: (a) The photon conversion into voltage inside the photodiode, (b) The stored data accuracy of the datalogger for this type of device, (c) The instrument variability in response to the optical filter temperature curve.

4.2.1. Sensors & amplifiers, optical filters and datalogger

The sensor element, which is compounded by a photodiode and the amplifier circuit is contained inside the collimation tube, together with the optical filter. The collimation tube was constructed of thermal insulating material, thus avoiding sharp fluctuations in temperature components, thus enabling measurements with lower uncertainty. A thermistor was inserted into one of the four collimation tubes in order to monitoring the internal temperature variation.

Small variations were noted in the internal temperature of the equipment during the mornings and afternoons during the measuring periods. These temperature variations affect the sensing element (photodiode) and the optical filter, hence contributing to uncertainty in the measured value.

Table 2
Local meteorological parameters at Caicó/Brazil during the campaigns.

	Dec. 2012				Sep. 2013			
Day	19	20	21	22	04	05	06	07
Temp. (°C) 10 am (UT)		30	31	30	27	29	29	28
Temp. (°C) 6 pm (UT)	37	36	36		35	35	34	35
RH (%) 10 am (UT)	55	55	53	52	65	57	56	57
RH (%) 6 pm (UT)	29	26	27		37	37	37	36
Atmosp. pressure (hPa) (average)	998	992	993	993	996	994	995	993

Source: Caicó – Climatology Station – INMET – Brazil

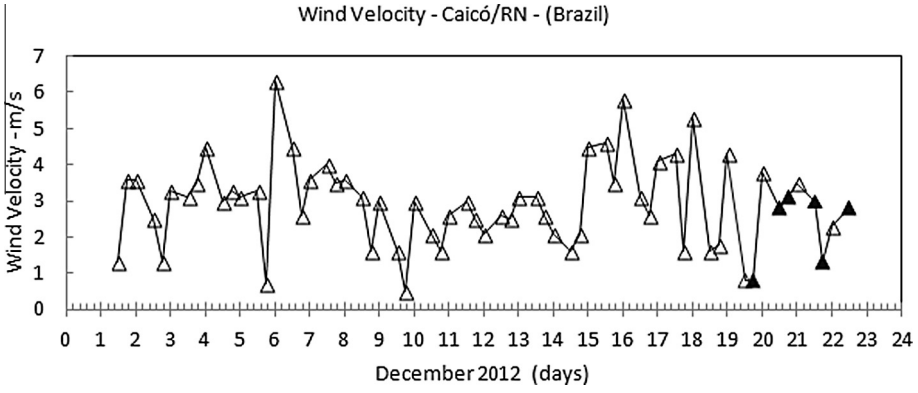

Fig. 4. Wind variability in Caicó – (▲) experiment days.

Variations in the internal temperature of the equipment followed the variation in outdoor temperature at the site, reaching the extreme values between $+29 \pm 1.0$ °C and $+35 \pm 1.0$ °C for the morning and afternoon periods respectively. Then the temperature variation (Δt) between morning and afternoon stood at 8 °C. In this case can be considered that the measured values uncertainty was within ±1.2% for the periods of measuring, or between morning and afternoon, for temperature variation (Δt) equal to 8 °C.

The optical filters have a range of bandwidth variation that change on temperature between 0.0017 and 0.025 nm/°C. With this temperature coefficient is possible to operate the device in a temperature range between 15 and 40 °C, without filter band displacement that could causes interference in the listed values for the calibration methodology application.

The CR10X datalogger was designed to work in temperatures ranging between 0 and 40 °C. Its 13 bits Analogical to Digital converter measures 2500 mV with full scale allows resolution of 333 μV. The accuracy of the equipment is at 0.1% for the full range of 2500 mV, i.e., an error of ±1.5 mV in the stored measurements. The worst situation occurs with the lower values obtained with the FSM-4 when the values are close to 300 mV, i.e., to the lowest intensity of the sun at sunrise and sunset are when the optical air mass is greater than 10. For this specific case the error introduced by the datalogger is less than ±0.5%.

4.2.2. Uncertainty in collected data

As shown in Section 3.1 the algorithm used to choose the collected valid value calculates the maximum values average over the time of one minute. The algorithm also discards the values below 1% of the highest value that can occur due to incorrect device pointing or interference of high altitude clouds. All graphs, generated in this work, has used solar radiation average values with at least 4 points with a standard deviation ±0.02%, out of this range the data is discarded. A similar algorithm used in AERONET network proposed by Smirnov et al. (2000) uses like primary criterion to indicate an atmospheric stability the analysis of the coefficient of variation using three measures (triplet) and CV > 1% are rejected.

Fig. 5 shows on September 7, 2013, the variability (SD%) of the values used in the average calculation using the SODDA VALG software, compared with the average value, i.e., the dispersion between the average value and the values used for its calculation.

Examining all the temperature effects over the FSM-4, i.e., the temperature effects in the photodiode conversion factor, other electronic devices, optical filters and

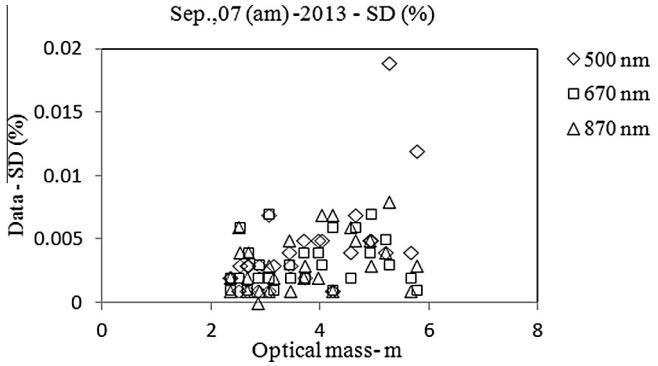

Fig. 5. Variability of the values used for estimating the averages compared with average values for all bands in Sep., 07 (am) 2013.

datalogger, an uncertainty smaller than ±1.2% in measurements is achieved.

4.3. Calculating the AOD

We fitted all collected data during the campaign periods to a linear function (least-square approach), separately for the morning (am) and afternoon (pm) data.

Fig. 6 shows, an example of the plot obtained with morning data sampling and respective fitted lines for bands in the visible (500 to 670 nm) and near infrared (870 nm) regions.

The total optical depth (τ_{total}), is given by the fitted line slope (Ichoku et al., 2002) and is inversely proportional to the radiation wavelength, i.e., when decreasing the radiation wavelength the absorption and scattering increases, due to aerosols present in the atmosphere. The wavelength dependency of the total optical depth (total) can be explained by the fact that the Rayleigh scattering as well as the aerosol optical thicknesses decrease with increasing wavelength.

Unlike aerosols, ozone causes absorption peaks in the visible spectrum (Chappuis band), with one peak at around 575 nm and another one at 603 nm, which reaches the maximum absorption in this band (Serdyuchenko et al., 2011).

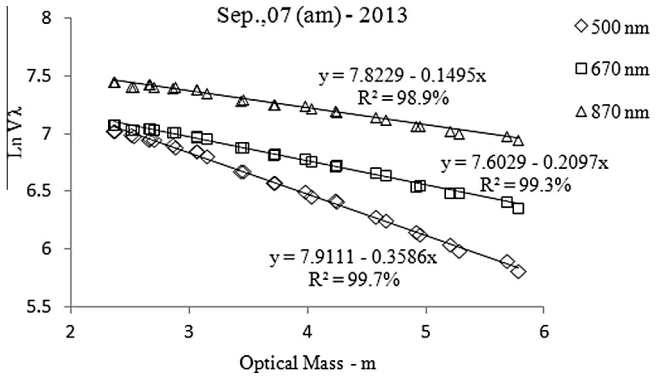

Fig. 6. Langley method applied to a morning data set and respective linear functions obtained by the least-square fits in Sep., 07 (am) 2013.

There is an exception to the bands where strong absorption of water vapor occurs, beginning in the near infrared. For these specific cases a higher optical depth value of the wave is obtained due to absorption by water molecules that are vaporized in the atmosphere.

More than 70% of the determination coefficient observed was bigger than 99% shown by the least squares fit line. Tables 3, 5 and 7 show the fitted line with their respective determination coefficient. Tables 4, 6 and 8 show the AODs, obtained from the observations made during December 2012 and September 2013, in the 500 nm, 670 nm and 870 nm bands. The determination coefficients to fitted lines are $R^2 \geqslant 99\%$, i.e., a very high correlation between the fitted lines and the collected data. Using Eq. (9) the AOD is calculated for each measurement period, according to results presented in Table 3.

There is a fluctuation in the AOD values during the first and second campaign, held in December 2012 and September 2013, respectively. The values obtained in the morning sets were generally higher than those ones obtained in the afternoon. Generally, higher AOD values are expected in the afternoon due to air convection caused by heating of the soil. This first verification of the AOD behavior at the measurement site indicates the variability of the local atmospheric opacity. This parameter is critical in order to determine whether the period of data measurement at the chosen site can be used in the calibration process.

The AOD values shown in Tables 4, 6 and 8 express average values as they are calculated during optical air mass variation in LM. In this case the uncertainty in the AOD is proportional to the determination coefficient of the fitted line, i.e., for higher determination coefficients less uncertainty in the AOD values was found. Once an instrument is calibrated with an extraterrestrial constant, valid instantaneous AOD data may be obtained.

A comparative with AERONET SPM using the average values of Petrolinás AOD and the FSM-4 AOD average data for Caicó, obtained for each single measuring period, proved to be unfeasible due to large discrepancies in the data. With more than 500 km of distance between the two sites, and the large spatial variability of AOD in the region, shown by satellite data, this inter-comparison became impracticable.

4.4. Calculation of the Angstrom coefficient

The Angstrom coefficient is a characteristic of the particles size distribution (Iqbal, 1983). The slope of the fitted line (or first derivative of the AOD) with wavelength is known as a logarithmic scale Angstrom coefficient (α).

In practice, the coefficient is calculated using two or more wavelengths, as shown in Eq. (13). Often between 500 and 870 nm are used:

$$\alpha(\lambda_1, \lambda_2) = -\left(\frac{\ln\left(\frac{\tau_{Aer,\lambda 1}}{\tau_{Aer,\lambda 2}}\right)}{\ln\left(\frac{\lambda_1}{\lambda_2}\right)}\right) \quad (13)$$

Table 3
Fitted line for 500 nm.

500 nm				
Day	Fitted line (b − ax)	R^2 (%)	Total optical depth $a \pm \sigma a$	(Ln V_0) $b \pm \sigma b$
Dec., 19 – 2012 (pm)	8.09 − 0.361x	99.3	0.361 ± 0.005	8.09 ± 0.02
Dec., 20 – 2012 (am)	7.97 − 0.401x	98.8	0.401 ± 0.006	7.97 ± 0.03
Dec., 20 – 2012 (pm)	7.92 − 0.334x	99.4	0.334 ± 0.004	7.92 ± 0.02
Dec., 21 – 2012 (am)	7.73 − 0.350x	99.2	0.350 ± 0.005	7.73 ± 0.03
Dec., 21 – 2012 (pm)	8.13 − 0.408x	99.2	0.408 ± 0.007	8.13 ± 0.03
Dec., 22 – 2012 (am)	7.95 − 0.366x	99.8	0.366 ± 0.002	7.95 ± 0.01
Sep., 04 – 2013 (pm)	7.69 − 0.238x	99.6	0.238 ± 0.002	7.690 ± 0.009
Sep., 05 – 2013 (am)	7.76 − 0.350x	99.6	0.350 ± 0.003	7.760 ± 0.016
Sep., 05 – 2013 (pm)	7.73 − 0.305x	98.9	0.305 ± 0.007	7.73 ± 0.02
Sep., 06 – 2013 (am)	7.879 − 0.356x	99.8	0.356 ± 0.003	7.879 ± 0.009
Sep., 07 – 2013 (am)	7.91 − 0.359x	99.7	0.359 ± 0.004	7.91 ± 0.02

Table 4
AOD calculation for 500 nm.

500 nm				
Day	Total optical depth	Ozone optical depth	Rayleigh	AOD (average)
Dec., 19 – 2012 (pm)	0.361	0.008	0.143	0.210
Dec., 20 – 2012 (am)	0.401	0.008	0.143	0.250
Dec., 20 – 2012 (pm)	0.334	0.008	0.143	0.183
Dec., 21 – 2012 (am)	0.350	0.008	0.143	0.199
Dec., 21 – 2012 (pm)	0.408	0.008	0.143	0.257
Dec., 22 – 2012 (am)	0.366	0.008	0.143	0.215
Sep., 04 – 2013 (pm)	0.238	0.008	0.143	0.087
Sep., 05 – 2013 (am)	0.305	0.008	0.143	0.154
Sep., 05 – 2013 (pm)	0.305	0.008	0.143	0.154
Sep., 06 – 2013 (am)	0.356	0.008	0.143	0.205
Sep., 07 – 2013 (am)	0.359	0.008	0.143	0.208

Table 5
Fitted line for 670 nm.

670 nm				
Day	Fitted line (b − ax)	R^2 (%)	Total optical depth $a \pm \sigma a$	Ln V_0 $b \pm \sigma b$
Dec., 19 – 2012 (pm)	7.99 − 0.206x	98.9	0.206 ± 0.003	7.99 ± 0.02
Dec., 20 – 2012 (am)	7.89 − 0.239x	97.7	0.239 ± 0.005	7.89 ± 0.02
Dec., 20 – 2012 (pm)	7.85 − 0.182x	99.0	0.182 ± 0.003	7.85 ± 0.01
Dec., 21 – 2012 (am)	7.71 − 0.197x	98.2	0.197 ± 0.005	7.71 ± 0.03
Dec., 21 – 2012 (pm)	7.98 − 0.228x	99.2	0.228 ± 0.004	7.98 ± 0.01
Dec., 22 – 2012 (am)	7.85 − 0.201x	99.5	0.201 ± 0.002	7.85 ± 0.01
Sep., 04 – 2013 (pm)	7.463 − 0.109x	99.6	0.109 ± 0.001	7.463 ± 0.004
Sep., 05 – 2013 (am)	7.5 − 0.209x	99.3	0.209 ± 0.003	7.50 ± 0.01
Sep., 05 – 2013 (pm)	7.47 − 0.161x	98.3	0.161 ± 0.004	7.47 ± 0.01
Sep., 06 – 2013 (am)	7.572 − 0.198x	99.7	0.198 ± 0.002	7.572 ± 0.006
Sep., 07 – 2013 (am)	7.6 − 0.210x	99.3	0.210 ± 0.003	7.60 ± 0.01

The α values greater than 2.0 indicate fine particles (smoke, sulfates), while an α near zero indicates the presence of mineral dust particles (Eck et al., 1999).

In this work, an Angstrom coefficient in the range of the 500 and 870 nm bands was calculated, (Table 9) indicating dust-like particles. The studied region is located in a semi-arid area and in situ measurements were carried out during the austral summer. The unique native Caatinga biome in the region can be described as a vegetation variation from savanna to wooded savanna. During this season of the year, the local vegetation loses its entire leafage. This leads to an increased radiation reaching the exposed soil, which in turn impacts on the wind patterns.

4.5. Methodology for V_0 variability analyses

The extraterrestrial constant V_0 behavior has been investigated evaluating the fitted line obtained with the

Table 6
AOD calculation for 670 nm.

670 nm				
Day	Total optical depth	Ozone optical depth	Rayleigh	AOD (average)
Dec., 19 – 2012 (pm)	0.206	0.012	0.044	0.150
Dec., 20 – 2012 (am)	0.239	0.012	0.044	0.183
Dec., 20 – 2012 (pm)	0.182	0.012	0.044	0.126
Dec., 21 – 2012 (am)	0.197	0.012	0.044	0.141
Dec., 21 – 2012 (pm)	0.228	0.012	0.044	0.172
Dec., 22 – 2012 (am)	0.201	0.012	0.044	0.145
Sep., 04 – 2013 (pm)	0.109	0.012	0.044	0.053
Sep., 05 – 2013 (am)	0.209	0.012	0.044	0.153
Sep., 05 – 2013 (pm)	0.161	0.012	0.044	0.105
Sep., 06 – 2013 (am)	0.198	0.012	0.044	0.142
Sep., 07 – 2013 (am)	0.210	0.012	0.044	0.154

Table 7
Fitted line for 870 nm.

870 nm				
Day	Fitted line (b – ax)	R^2 (%)	Total optical depth $a \pm \sigma a$	Ln V_0 $b \pm \sigma b$
Dec., 19 – 2012 (pm)	7.85 – 0.135x	97.9	0.135 ± 0.003	7.85 ± 0.01
Dec., 20 – 2012 (am)	7.83 – 0.166x	95.5	0.166 ± 0.005	7.83 ± 0.02
Dec., 20 – 2012 (pm)	7.75 – 0.116x	98.9	0.116 ± 0.002	7.75 ± 0.01
Dec., 21 – 2012 (am)	7.69 – 0.130x	97.5	0.130 ± 0.004	7.69 ± 0.02
Dec., 21 – 2012 (pm)	7.88 – 0.155x	98.3	0.155 ± 0.004	7.88 ± 0.01
Dec., 22 – 2012 (am)	7.79 – 0.131x	99.3	0.131 ± 0.002	7.79 ± 0.01
Sep., 04 – 2013 (pm)	7.673 – 0.054x	96.5	0.054 ± 0.002	7.673 ± 0.007
Sep., 05 – 2013 (am)	7.72 – 0.147x	98.3	0.147 ± 0.003	7.72 ± 0.01
Sep., 05 – 2013 (pm)	7.71 – 0.108x	95.9	0.108 ± 0.005	7.71 ± 0.01
Sep., 06 – 2013 (am)	7.779 – 0.129x	98.5	0.129 ± 0.003	7.779 ± 0.009
Sep., 07 – 2013 (am)	7.82 – 0.150x	98.9	0.150 ± 0.003	7.82 ± 0.01

Table 8
AOD calculation for 870 nm.

870 nm				
Day	Total optical depth	Ozone optical depth	Rayleigh	AOD (average)
Dec., 19 – 2012 (pm)	0.135	0	0.015	0.120
Dec., 20 – 2012 (am)	0.166	0	0.015	0.151
Dec., 20 – 2012 (pm)	0.116	0	0.015	0.101
Dec., 21 – 2012 (am)	0.130	0	0.015	0.115
Dec., 21 – 2012 (pm)	0.155	0	0.015	0.140
Dec., 22 – 2012 (am)	0.131	0	0.015	0.116
Sep., 04 – 2013 (pm)	0.054	0	0.015	0.039
Sep., 05 – 2013 (am)	0.147	0	0.015	0.132
Sep., 05 – 2013 (pm)	0.108	0	0.015	0.093
Sep., 06 – 2013 (am)	0.129	0	0.015	0.114
Sep., 07 – 2013 (am)	0.150	0	0.015	0.135

collected data, showing the V_0 tendency in the December 2012 and September 2013 campaigns. We compare different V_0 values achieved on each half day, to the found V_0 variation using equation 18 embedded in and a small computer routine. Similar methodology was used by Kaufman and Fraser (1983) to check the sun radiation extinction by aerosols, trying to identify the aerosol dominant parameter and comparing some meteorological data, such as surface visibility, relative humidity and temperature profile. In this present work we use the Kaufman and Fraser methodology, observing the behavior of AOD by variation of the linear coefficient (ΔV_0) in line fitting. The optical depth is derived for each wavelength by measuring the voltage produced by the photodiode using Eq. (14):

$$\tau = \left(\ln \frac{V}{V_0}\right)\frac{1}{m} \tag{14}$$

The optical air mass is given by m, while V_0 is the calibration constant of the device. The uncertainty of the calibration constant V_0 is caused by the variation of the optical

Table 9
Angstrom values during campaigns days.

Angstrom 500/870 nm	
Dec., 19 (pm) – 2012	1.010
Dec., 20 (am) – 2012	0.910
Dec., 20 (pm) – 2012	1.073
Dec., 21 (am) – 2012	0.990
Dec., 21 (pm) – 2012	1.097
Dec., 22 (am) – 2012	1.114
Sep., 04 (pm) – 2013	1.449
Sep., 05 (am) – 2013	0.278
Sep., 05 (pm) – 2013	0.911
Sep., 06 (am) – 2013	1.059
Sep., 07 (am) – 2013	0.780

Table 10
AOD dependence of the $\Delta V_0/V_0$ variation.

Optical mass	$\Delta V_0/V_0$ (%)				
	0.5%	1%	2%	3%	
1	0.005	0.01	0.02	0.03	AOD Incertainty
2	0.0025	0.005	0.01	0.015	
3	0.0022	0.003	0.007	0.01	
4	0.002	0.0025	0.005	0.007	
5	0.001	0.002	0.003	0.006	

depth, and m is given by lower mass value of the optical segment under consideration in Eq. (15):

$$\Delta\tau = \frac{\Delta V_0}{V_0}\frac{1}{m} \tag{15}$$

The sites regularly used for sun photometer calibration by the Langley method measured data on clear days, i.e., with few aerosols (low AOD). The linear coefficient (V_0) variation shows the variation of optical depth, where the largest spatial and temporal variation is due to aerosols. The V_0 uncertainty is given by $\Delta V_0/V_0$ fluctuations, and can be calculated using Eq. (16):

$$\frac{\Delta V_0}{V_0} = \frac{|V_{02} - V_{01}|}{V_{01}} \tag{16}$$

This behavior analysis of the collected data, from the first and second campaign, in December 2012 and September 2013, respectively, are shown in Tables 11–13. All data in the tables are converted from ln V_0 to V_0. This methodology allows for estimating the V_0 variation, and is therefore a measure of the instrument's calibration error (Kaufman and Fraser, 1983).

The uncertainty depends on the variation of the optical air mass and $\Delta V_0/V_0$, as show the error curves which decrease for large optical air masses showed in Table 10 (Porter et al., 2001). In our case we expected to obtain a $\Delta V_0/V_0$ ratio near 2% with optical air mass variation between 1 and 5.

Tables 11–13 show different V_0 absolute values with lowest variation of $\Delta V_0/V_0$ divided in values groups (A, B, C and D) for 670 and 870 nm and values groups (A and B) for 500 nm. Each group aggregates measurements with similar values of the V_0. We show the combinations of each half day of measurements with smallest variations of less than 3.6% of $\Delta V_0/V_0$ which is near the lower limit of uncertainty when using a laboratory calibration camera. It can be noted that the variation of $\Delta V_0/V_0$ reached the desirable values in all three bands studied. With the results achieved with the combination of eleven half days of measurements, distributed between the months of December 2012 and September 2013, we found better values than the laboratory calibration. However, the constant V_0 presented changes due to variability of the AOD.

The differing values are sub-divided in different groups that show the dependence of ΔV_0 with the variation of $\Delta\tau(t)$, according to Shaw (1979). It is a challenge to find atmospheric stability with high AOD values measured at low altitude sites, compared to those found at high altitude sites. Repetition of the high value for several days is an extremely rare, however possible condition, as shown by Liu et al. (2011). According to Shiobara et al. (1996), only if the V_0 value is repeated during several days of independent measurements, it can be regarded as reliable. A possible correlation of the AOD variability with meteorological conditions, such as the wind or surface temperature, was not found because the meteorological data needs to be acquired in short time steps to achieve a correct proof of correlation.

We can note that the best days for $\Delta V_0/V_0$ with acceptable values for calibration (less than 3.6%) in a specific band are not necessarily the same for other bands, i.e., the best $\Delta V_0/V_0$ occurred on different days with different bands. For the 500 and 870 nm bands we obtained the

Table 11
The best results of $\Delta V_0/V_0$ variation for 500 nm.

500 nm				
Day	V_{01}	V_{02}	$\Delta V_0/V_0$ (%)	
Dec., 20 (am) – 2012, Dec., 22 (am) – 2012	2892.9	2835.6	2.0	A
Dec., 20 (pm) – 2012, Dec., 22 (am) – 2012	2751.8	2835.6	3.0	
Dec., 20 (pm) – 2012, Sep., 07 (am) – 2013	2751.8	2724.39	1.0	
Sep., 06 (am) – 2013, Sep., 07 (am) – 2013	2641.23	2724.39	3.1	
Dec., 21 (am) – 2012, Sep., 05 (am) – 2013	2275.6	2344.9	3.0	B
Dec., 21 (am) – 2012, Sep., 05 (pm) – 2013	2275.6	2275.6	0.0	
Sep., 05 (am) – 2013, Sep., 05 (pm) – 2013	2344.9	2275.6	3.0	

Table 12
The best results of $\Delta V_0/V_0$ variation for 670 nm.

670 nm				
Day	V_{01}	V_{02}	$\Delta V_0/V_0$ (%)	
Dec., 19 (pm) – 2012, Dec., 21 (pm) – 2012	2951.3	2921.93	1.0	A
Dec., 20 (pm) – 2012, Dec., 22 (am) – 2012	2565.73	2565.73	0.0	B
Sep., 04 (pm) – 2013, Sep., 05 (am) – 2013	1742.37	1808.04	3.6	C
Sep., 05 (am) – 2013, Sep., 05 (pm) – 2013	1808.04	1754.61	3.0	
Sep., 06 (am) – 2013, Sep., 07 (am) – 2013	1943.02	1998.2	2.8	D

Table 13
The best results of $\Delta V_0/V_0$ variation for 870 nm.

870 nm				
Day	V_{01}	V_{02}	$\Delta V_0/V_0$ (%)	
Dec., 19 (pm) – 2012, Dec., 20 (am) – 2012	2565.734	2514.929	2.0	A
Dec., 19 (pm) – 2012, Dec., 21 (pm) – 2012	2565.734	2643.873	3.0	
Dec., 19 (pm) – 2012, Sep., 07 (am) – 2013	2565.734	2489.905	3.0	
Dec., 20 (am) – 2012, Sep., 07 (am) – 2013	2514.929	2489.905	1.0	
Dec., 20 (pm) – 2012, Sep., 05 (am) – 2013	2321.572	2252.96	3.0	B
Dec., 20 (pm) – 2012, Sep., 06 (am) – 2013	2321.572	2389.884	2.9	
Sep., 05 (am) – 2013, Sep., 05 (pm) – 2013	2252.96	2230.542	1.0	
Dec., 21 (am) – 2012, Sep., 04 (pm) – 2013	2186.375	2149.52	1.7	C
Dec., 21 (am) – 2012, Sep., 04 (pm) – 2013	2186.375	2149.52	1.7	
Dec., 22 (am) – 2012, Sep., 06 (am) – 2013	2416.318	2389.884	1.1	D
Dec., 22 (am) – 2012, Sep., 07 (am) – 2013	2416.318	2489.905	3.0	

highest number of combined days while the 670 nm band showed just four acceptable results. It was observed that the R^2 coefficient that was over 98% on most days of measurements, indicated a locally stable atmosphere during each half of the sampled days. However, the fluctuation of the measured AOD average in the two half days detracted the values obtained for V_0. As the site is located at low altitude it is more prone to higher values of AOD and thus yields a higher variability, which is not desirable for calibration purposes.

SPM can be calibrated in a laboratory using ISS (Integrating Sphere Sources) that simulates the sunlight. The results of the laboratory calibration keep the instrument with an uncertainty between 5% and 3%. All instruments are routinely calibrated with Goddard's two meter integrating sphere at GSFC (Goddard Space Flight Center) at least twice per year and the reference instruments are calibrated approximately monthly. Each calibration session consists of three sequential measurements at four lamp levels (radiance levels). The sphere's precision is not well known however the absolute accuracy is ~5% or less. According to NIST (National Institute for Standard and Technology), a north American government institute who trace calibration using the ISS at GSFC/NASA, the uncertainties in this kind of measurements could reach maximum values of 5% (Pietras et al., 2001).

In the study conducted by Kaufman and Fraser (1983), data for optical depth analysis with a sun photometer were collected during three days using the Langley method. Samples were collected at GSFC/NASA located 20 km away from Washington – DC, thus close to pollution sources, which are intensified in summer. Cleaner air days were chosen during the summers of 1980 and 1981. In the setting of lines to the collected data for the calculation of the V_0 error, $\Delta V_0/V_0 = 0.03$ (3%) was obtained. For Mauna Loa – Hawaii, USA, which is a place of exceptional quality condition for these measurements, values are found at $\Delta V_0/V_0 = 0.005$ (0.5%). According to Holben et al. (1998) the variability of V_0 for the visible and near-infrared band should be between 0.25% and 0.5%.

The SPM calibration work performed by Schmid and Wehrli (1995) at Jungfraujoch, which is also a site of great quality for this kind of purpose, brought excellent results and was based on data collected in four consecutive months, going from September to December 1993. Schmid and Wehrli (1995) show that, despite the superior results provided by the LM with longer campaigns, the use of such additional calibration laboratory methods is important to monitor the instrument degradation.

We plan future campaigns with an expanded number of experiment days, allowing a greater number of ideal clear days. In addition, it will allow an improved characterization of the site in the region of Caicó/RN to better understand the variability of AOD.

5. Conclusions

Two measurement campaigns were carried out close to the city of Caicó during the summer season, in the semiarid region of northeastern Brazil, to characterize aerosol

optical depth variability using the Langley method. The data obtained in these first campaigns show high variability of optical depth, even though the site being located relatively far from anthropogenic aerosols emission sources. Comparative tests carried out between the Langley coefficients obtained for the various half days of measurements reveal the expected results (with $\Delta V_0/V_0$ values less than 3.6%) for four half days for the 670 nm band, and for five and six days in the 500 and 870 nm bands, respectively. However, these results occur in two or three different ranges of V_0 values, which does not represent the ideal situation. According to Shaw (1979) the optical depth usually changes its values in time following aerosol fluctuation, i.e., variation of $\Delta\tau(t)$, causing errors in the calibration process when its temporal dependence is ignored.

The line fitted to the data show very high coefficients of determination, with maxima of 99.80%, 99.50% and 99.32%, in the bands 500, 670 and 870 nm, respectively during the two campaigns. However, the methodology for verification of the constant V_0's variability, reflected as the slopes of the fitted line in the various studied optical air mass ranges showed variations, which indicates fluctuations in optical depth levels.

The region has no significant emission sources of anthropogenic aerosols to influence the local atmosphere. Therefore, the AOD fluctuation is of natural origin for the period of the measurements, for example due to dry vegetation that loses its leafs leading to the intensification of winds: wind velocity increases due to lower surface roughness coupled with a stronger convection of air masses due to higher soil temperatures. Both processes contribute to the increase of particle injection into the atmosphere and thus a high variability of AOD. We expected higher AOD values during the afternoon due to increased air convection, but observed more days during the morning with higher AOD. The full explanation of this phenomenon requires further measurements for longer periods of time to fully understand the underlying processes.

The high AOD variability found during these two short campaigns indicate that the site may not be the most adequate for SPM calibration. However, longer campaigns may yield a more complete picture: The site needs to be characterized with more conclusive results about the suitability of its use for calibration of SPM's. More research needs to be done in the region to confirm the present AOD data with the same methodology helping to identify possible sources causing AOD variability.

The realization of new campaigns during other periods of the year is already envisioned and will contribute to a more comprehensive characterization of AOD variability in the semiarid region. We expect that the variation of V_0 in other times of the year will reach values between 0.01 (1%) and 0.02 (2%), ensuring an uncertainty compatible with similar portable sun photometers. Periods will be chosen with appropriate atmospheric conditions, i.e., clear skies, clean air and mild temperatures, after the rainy season. An alternative to check the FSM-4 calibration will be to make in situ measurements at the AERONET site in Petrolina – Brazil, proceeding with transfer calibration using the inter-calibration methodology (e.g., Porter et al., 2001).

In the near future we plan to create a small regional network of reliable and cheap sun photometers to obtain a comprehensive view of AOD behavior in the area. Another purpose for this regional network will be providing data for validation of AOD satellite algorithms.

Acknowledgments

The authors thank the INPE/CRN (National Institute for Space Research/Northeast Regional Center) for the support to use their laboratories for assembly and testing of prototypes, and providing transportation for campaigns; We also thank the anonymous reviewers of this paper who contributed substantially to improve the presentation of our study. We thank the AEB (Brazilian Space Agency) for funding the project: "Determinação do Perfil Vertical de Variáveis Atmosféricas no Rio Grande do Norte para Validação de Dados obtidos por Satélites": DEPVARN – SAT, edital AEB/MCT/CNPq No 033/2010 Processo n° 560314/2010-8.

References

Alexandrov, M.D., Kiedron, P., Michalsky, J.J., Hodges, G., Flynn, C.J., Lacis, A.A., 2007. Optical depth measurements by shadow-band radiometers and their uncertainties. Appl. Opt. 46 (33).

Bodhaine, B.A., Wood, N.B., Dutton, E.G., Slusser, J.R., 1999. On Rayleigh Optical Depth Calculations. J. Atmos. Ocean. Technol. 1. American Meteorological Society.

Bruegge, C.J., Conel, J.E., Green, R.O., Margolis, J.S., Holm, R.G., Toon, G., 1992. Water vapor column abundance retrievals during FIFE. J. Geophys. Res. 97 (18), 18759–18768.

Dutton, E.G., Reddy, P., Ryan, S., DeLuisi, J.J., 1994. Features and effects of aerosol optical depth observed at Mauna Loa, Hawaii: 1982–1992. J. Geophys. Res. 99 (D4), 8295–8306. http://dx.doi.org/10.1029/93JD03520.

Eck, T.F., Hoben, B.N., Reid, J.S., Dubovick, O., Smirnov, A., O'Neill, N.T., Slutsker, I., Kinne, S., 1999. Wavelength dependence of optical depth of biomass burning, urban and desert dust aerosols. J. Geophys. Res. 104, 31333–31350.

Green, A.E.S., 1964. Attenuation by ozone and the earth's albedo in the middle ultraviolet. Appl. Opt. 3 (2), 203–209.

Halthore, R.N., Schwartz, S.E., Michalsky, J.J., Anderson, G.P., Ferrare, R.A., Holben, B.N., Brink, H.M., 1997a. Comparison of model estimated and measured direct-normal solar irradiance. J. Geophys. Res. 102, 29991–30002.

Halthore, R.N., Eck, T.F., Holben, B.N., Markhan, B.L., 1997b. Sunphotometric measurements of atmospheric water vapor column abundance in the 940 nm band. J. Geophys. Res. 102 (D4), 4343–4352.

Harrison, L., Michalsky, J., Berndt, J., 1994. Automated multifilter rotating shadow-band radiometer: an instrument for optical depth and radiation measurements. Appl. Opt. 33, 5118–5125.

Holben, B.N., Eck, T.F., Slutsker, I., Tanre, D., Buis, J.P., Setzer, A., Vermote, E., Reagan, J.A., Kaufman, Y., Nakagima, T., Lavenu, F., Jankowiak, I., Smirnov, A., 1998. AERONET – a federated instrument network and archive for aerosol characterization. Rem. Sens. Environ. 66, 1–16.

Ichoku, C., Levy, R., Kaufman, Y.J., Remer, L.A., Li, R.-R., Martins, V.J., Holben, B.N., Abuhassan, N., Slutsker, I., Eck, T.E., Pietras, C.,

2002. Analysis of the performance characteristics of the five-channel Microtops II Sun photometer for measuring aerosol optical thickness and precipitable water vapor. J. Geophys. Res. 107 (D13).
Iqbal, M., 1983. An Introduction to Solar Radiation. Academic Press, 390.
Kasten, F., 1966. A new table and approximate formula for relative optical air mass. Arch. Meteor. Geophys. Bioklim. B14, 206–223.
Kasten, F., Young, A.T., 1989. Revised optical air mass tables and approximation formula. Appl. Opt. 28, 4735–4738.
Kaufman, Y.J., 1993. Aerosol Optical Thickness and Atmospheric Path Radiance. J. Geophys. Res. 98 (D2), 2677–2692.
Kaufman, Y.J., Fraser, R.S., 1983. Light extinction by aerosols during summer air pollution. J. Clim. Appl. Meteorol. 22, 1694–1706. American Meteorological Society.
Kobayashi, T., 1981. The design of a new sun photometer and some considerations on Langley calibration. Meteorol. Geophys. 32 (2), 79–88.
Liou, K.N., 2002. An Introduction to Atmospheric Radiation, second ed. Academic Press, p. 579.
Liu, C., Li, Y., Gao, W., Shi, R., Bai, K., 2011. Retrieval of columnar water vapor using measurements over northern China. J. Appl. Remote Sens. 5.
McArthur, B.L.J., Halliwell, D.H., Niebergall, O.J., O'Neill, N.T., Slusser, J.R., Wehrli, C., 2003. Field comparison of network Sun photometers. J. Geophys. Res. 108 (D19), 4596. http://dx.doi.org/10.1029/2002JD002964.
Michalsky, J.J., 1988. The astronomical almanac's algorithm for approximate solar position (1950–2050). Sol. Energy 40 (3), 227–235, USA.
Osterwald, C.R., Emery, K.A., 2000. Spectroradiometric Sun photometry. J. Atmos. Ocean. Technol. 17, 1171–1188.
Pietras, C., Miller, M., Frouin, R., Eck, T., Holben, B., Marketon, J., 2001. Calibration of Sun photometers and sky radiance sensors. In: Barnes, R., Fargion, G.S., McClain, C. (Eds.), In Situ Aerosol Optical Thickness Collected by the SIMBIOS Program 1997–2000: Protocols, and Data QC and Analysis. NASA, Goddard Space Flight Center, Greenbelt, MD.
Porter, J.N., Miller, M., Pietras, C., Motell, C., 2001. Ship-based Sun photometer measurements using microtops Sun photometers. J. Atmos. Ocean. Tech. 18, 765–774.
Reagan, J.A., Thome, K., Herman, B., Gall, R., 1987. Water vapor measurement in 0.94 micro absorption band: calibration, measurements, and data applications. In: Reagan, J.A. (Ed.), Proceedings of International Geoscience and Remote Sensing Symp.'87 Symposium. University of Michigan, Ann Arbor, 63–57.
Reagan, J.A., Thome, K., Herman, B.M., 1992. A Simple instrument and technique for measuring columnar water vapor via near-IR differential solar transmission measurements. IEEE Trans. Geosci. Remote Sens. 30 (4).
Robinson, N., 1966. Solar Radiation. Elsevier, New York, 347 pp.
Rollin, E.M., 2000. An introduction to the use of Sun-photometry for the atmospheric correction of airborne sensor data. In: Annual Meeting of the Users of the NERC Airborne Remote Sensing Facility (NERC ARSF), Keyworth, Nottingham, UK.
Sahai, Y., Kirchhoff, V.W., Paes Leme, N.M., 2000. Equatorial and low latitude total ozone measurements in Brazil. In: Quadrennial Ozone Symposium, 2000, Sapporo, Japan, pp. 619–620.
Schmid, B., Wehrli, C., 1995. Comparison of sun photometer calibration by use of the Langley technique and the standard lamp. Appl. Opt. 34 (21).
Serdyuchenko, A., Gorshelev, V., Weber, M., Burrows, J.P., 2011. New broadband high-resolution ozone absorption cross-sections. Spectrosc. Eur. 23 (6), 14–17.
Shaw, G.E., 1979. Sun photometry atmospheric ozone: determination by Chappuis band absorption. J. Appl. Meteorol. Am. Meteor. Soc., 1335–1339.
Shaw, G.E., 1983. Sun photometry. Bull. Am. Meteor. Soc. 64, 4–11.
Shiobara, M., Spinhirne, J.D., Uchiyama, A., Shoji, Asano, 1996. Optical depth measurements of aerosol cloud, and water vapor using sun photometers during fire cirrus IFO II. J. Appl. Meteor. 35, 36–46.
Silva, A.A., Kirchhoff, V.W., 2004. Aerosol optical thickness from Brewer spectrophotometers and an investigation into the stray-light effect. Appl. Opt. 43 (12).
Slusser, J., Gibson, J., Biglow, D., 2000. Langley method of calibrating UV filter radiometers. J. Geophys. Res. 105, 4841–4849.
Smirnov, A., Holben, B.N., Eck, T.F., Dubovik, O., Slutsker, I., 2000. Cloud-screening and quality control algorithms for the AERONET database. Remote Sens. Environ. 73, 337–349.
WMO – N°. 8, 2008. Guide to Meteorological Instruments and Methods of Observation, seventh ed., ISBN 978-92-63-10008-5.
Young, A.T., 1981. On Rayleigh-Scattering optical depth of atmosphere. J. Appl. Meteorol. 20, 328–330.